Band unpinning and photovoltaic model for P3HT:PCBM organic bulk heterojunctions under illumination

Juan Bisquert [a,*], Germà Garcia-Belmonte [a], Antoni Munar [a], Michele Sessolo [b], Alejandra Soriano [b], Henk J. Bolink [b]

[a] Departament de Física, Universitat Jaume I, 12071 Castelló, Spain
[b] Institut de Ciència Molecular, Universitat de València, Polígon La Coma s/n, 46980 Paterna, València, Spain

ARTICLE INFO

ABSTRACT

Capacitance analysis of P3HT:PCBM bulk heterojunction solar cells, in dark and under illumination, shows a linear Mott–Schottky characteristic at moderate reverse bias, indicating p-doping of the organic blend. The flatband potential under illumination is displaced negatively about 0.6 V with respect to dark conditions. A basic photovoltaic model is developed to explain this, in terms of electron transfer via surface states at the metal/organic interface. Surface states with a slow exchange kinetics, become charged under illumination, unpinning the band and decreasing the depletion layer at the electron extraction contact. This becomes a major factor limiting the performance of bulk heterojunction solar cells.

© 2008 Elsevier B.V. All rights reserved.

1. Introduction

Bulk heterojunctions formed by an interpenetrating blend of an optically active polymer and electron accepting molecules constitute a very promising route towards cheap and versatile solar cells [1]. The combination of poly(3-hexylthiophene) (P3HT) and [6,6]-phenyl C61-butyric acid methyl ester (PCBM) in organic blends has recently shown high photovoltaic performance [2]. P3HT displays a relatively high hole mobility ($\sim 10^{-4}$ to 10^{-3} cm^2 V^{-1} s^{-1}) [3] and it was shown that P3HT:PCBM blends exhibit a remarkable improvement of performance when annealed, due to better ordering of the polymer phase that enhances the hole conductivity [4,5]. Another important factor determining performance is the offset between the polymer HOMO level and the fullerene LUMO level, since that separation provides an upper limit to the photovoltage. Studies indicate the formation of a dipole as large as 0.6 eV at the interface between the two organic materials [6].

It is also recognized that P3HT can easily undergo p-doping when exposed to air or moisture [7–10], the doping level being related to the oxygen concentration in the polymer film. The p-doping opens the possibility of the formation of a Schottky barrier at the contact, which eventually may play an important role in carrier extraction. Recently, we showed that such a barrier can be detected by capacitance techniques in P3HT:PCBM blends [11], indeed a typical Mott–Schottky characteristic (MS, linear C^{-2} vs. V) is observed at reverse bias in the dark conditions. Previous studies [12] have found the MS characteristic in P3HT and the relation to the level of oxygen doping.

It is well known that in a Schottky barrier the voltage across the metal–semiconductor interface is divided in two contributions, the space-charge region (SCR) in the semiconductor and the dipole layer in the surface. The latter layer may consist of a thin oxide layer in inorganic contacts [13,14] or a double layer in semiconductor–electrolyte contacts [15]. In general the dipole layer is characterized by a constant capacitance. Since this capacitance absorbs part of the voltage, there is a shift of the conduction band energy at the interface, implying that the barrier for electron transfer, as indicated by the intercept of the MS plot, is less than the difference of work functions between the contacting materials. Surface states at the metal semiconductor interface are known to determine many aspects of the electrical behavior of the Schottky barrier [16–18]. First, surface states produce a sheet of electrical charge that modifies the electrostatic equilibrium of the interface. In addition, surface states, lying lower in energy than the conduction band states, often provide a preferential kinetic path for electron transfer from the semiconductor to the contact material. An important effect of the presence of surface states was observed in the photoelectrochemistry of semiconductor electrodes [15,19–21]. Under illumination, the concentration of minority carriers increases at the contact, with respect to the dark conditions. Thus at the same external voltage, the surface state acquires more charge under illumination, and the flatband potential determined from the MS plot changes [15]. In effect parallel MS plots are observed at different illumination light intensities [15,19–21]. Steady state models considering the band shift due to the surface state occupancy have been formulated [19,22].

Continuing our previous research on MS analysis of organic blends [11], we have analyzed the $C - V$ characteristics of ITO/PEDOT:PSS/P3HT:PCBM/Al solar cells both in dark and under illumination and we observed a considerable (0.6 V) displacement

* Corresponding author. Fax: +34 964 728 066.
E-mail address: bisquert@fca.uji.es (J. Bisquert).

of the MS plots under illumination with respect to the dark characteristic, which slowly decreases again to its previous value in dark when the light is turned off. This will be interpreted in terms of the properties of the P3HT:PCBM-Al contact, and we propose that surface states at the metal–organic interface introduce important effects determining the kinetics and energetics of the electron-extracting contact of the solar cell. In Section 2 of this paper we formulate a model for steady state conditions of the solar cell that is able to explain the modification of the barrier under illumination. The model is based on a well known approach, i.e. the Gärtner model [23] that combines diffusion of minorities in the neutral zone and complete collection at the SCR. The flux of minority carriers at the interface is coupled to the kinetics of the interfacial surface states [24]. However, a number of factors are taken into account for the suitable application of the model in organic blends:

(a) The kinetics of charge transfer at the metal–organic interface is described in terms of an injection model recently developed for luminescent organic devices [25–28]. This model is already based on the idea of the displacement of a surface state (mediating charge transfer across the interface) as a function of bias, and has given very good results for describing capacitance characteristics at forward bias.
(b) In order to characterize in detail the photovoltaic properties of the organic blend, the model must describe self-consistently the relationship of charge in the surface state to the potential distribution in the dipole layer and the SCR [18,29].
(c) Since the photoactive region is usually very thin, one to a few hundred nanometers, specific boundary conditions are used to solve the diffusion–generation recombination equation in a spatially restricted photoactive layer.
(d) In classical photoelectrochemical systems the SCR usually receives direct illumination and forms the main charge collection interface. In organic P3HT:PCBM solar cells, so far doping is an uncontrolled process and it was found [11] that the dominant barrier is at the opaque electrode, the P3HT:PCBM-Al contact. For generality, we derive the model for illumination from either side of the solar cell. If the light is predominantly absorbed in the neutral region of the semiconductor, charge collection relies on a long diffusion length of the separate charge carriers, as in dye-sensitized solar cells [30,31].

By combining these elements, we provide a model for carrier generation, collection, and transference across the interface, that emphasizes the importance of recombination due to limitations of charge-transfer kinetics [24], and allows to predict the energetics of the barrier in any set of conditions of applied voltage and photon irradiation. Section 3 provides the methods of preparation and measurement of the organic blends, and Section 4 presents the experimental results as well as the discussion in terms of the proposed mechanism.

2. Model

2.1. Energetics

The energy diagram assumed in the model is shown in Fig. 1a, and a list of the symbols used is given in Table 1. The barrier in the SCR is included in the model as the potential drop V_{sc}. In addition we assume a potential drop V_d at the dipole layer at the metal/organic interface. In terms of local values of the electrostatic potential (ϕ), we have

$$V_{sc} = \phi_s - \phi_{sc,b} \tag{1}$$

$$V_d = \phi_m - \phi_s \tag{2}$$
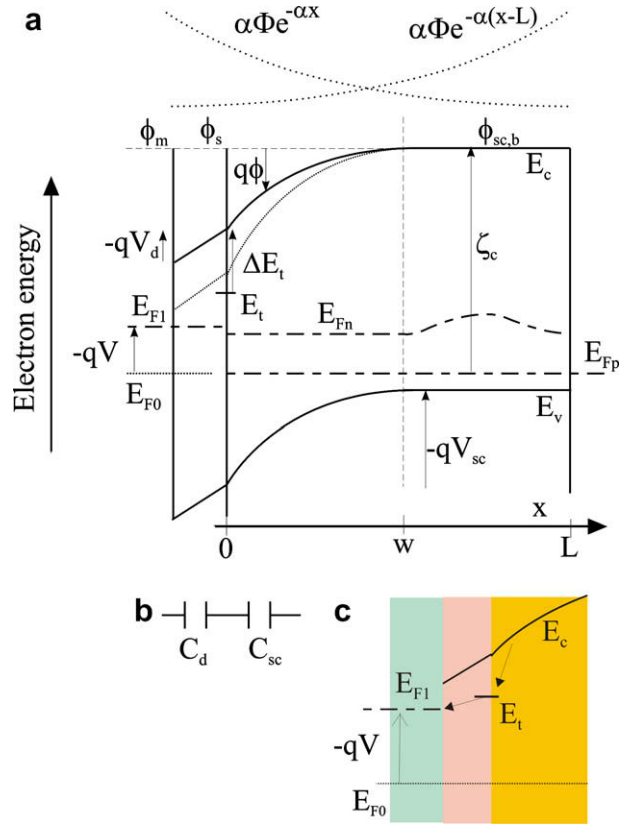
Fig. 1. (a) Scheme of a BHJ solar cell showing the space-charge region, a dipole layer, and a surface state at the metal/organic interface. Symbols are defined in Table 1. On top is shown the photogeneration profiles for illumination both from barrier and from the neutral sides. (b) The capacitances of dipole layer and SCR. (c) Steps of electron extraction through surface states.

The built-in potential is

$$V_{bi} = \phi_{sc,b,eq} - \phi_{m,eq} \tag{3}$$

And the applied potential is

$$V = \phi_m - \phi_{m,eq} - (\phi_{sc,b} - \phi_{sc,b,eq}) \tag{4}$$

Combining Eqs. (1)–(4) we obtain

$$V = V_{bi} + V_d + V_{sc} \tag{5}$$

On the other hand we have in terms of Fermi levels

$$E_{F1} - E_{F0} = -qV \tag{6}$$

and $E_{Fp} = E_{F0}$. The size of the depletion layer in the semiconductor is

$$w = w_0 V_{sc}^{1/2} \tag{7}$$

where

$$w_0 = \left(\frac{2\varepsilon}{qN_A}\right)^{1/2} \tag{8}$$

Here $\varepsilon = \varepsilon_r \varepsilon_0$. The capacitance of the depletion layer is

$$C_{sc} = \frac{\varepsilon}{w_0 V_{sc}^{1/2}} \tag{9}$$

The capacitance in the dipole layer C_d is assumed constant. Since the surface state at fractional occupancy θ obtains a charge $N_l q\theta$, the electrostatic equilibrium across the interface consists of two capacitors in series with excess charge in the central plates (see Fig. 1b) [18,29], hence

Table 1
List of symbols used in the text

q	The positive elementary charge
k_BT	The thermal energy
E_{F0}	The equilibrium Fermi level [0 eV]
E_{F1}	The Fermi level in the metal
E_{Fn}	The quasi-Fermi level of electrons
E_{Fp}	The quasi-Fermi level of holes
w	Width of the depletion layer
V	The potential applied at the barrier contact
V_d	The potential drop across the dipole layer
V_{sc}	The potential drop across the organic layer (bandbending)
V_{bi}	The built-in potential [−0.4 eV]
ϕ	The local potential
ϕ_m	The local potential in the metal
ϕ_s	The local potential at the metal/organic interface
ϕ_m	The local potential in the metal
ε	Dielectric constant of the organic layer
ε_r	Relative dielectric constant of the organic layer [3]
ε_0	Permittivity of vacuum [8.85×10^{-14} F cm^{-1}]
C_0	Low-frequency capacitance
C_d	Capacitance of the dipole layer [2×10^{-7} F cm^{-2}]
C_{sc}	Capacitance of the depletion layer
D_n	Electron diffusion coefficient [2×10^{-5} cm2 s^{-1}]
L_n	Electron diffusion length [300 nm]
α	Light absorption coefficient [5×10^{-3} nm^{-1}]
Φ	Incident photon intensity [0, 10^{15} cm^{-2}]
E_c	The LUMO in the organic conductor
ζ_c	Deepness of the bulk Fermi level for electrons in equilibrium, with respect to E_c
N_c	The total density of states (per unit volume) in the bulk LUMO [10^{21} cm^{-3}]
N_A	The acceptor doping density in the organic layer [5×10^{16} cm^{-3}]
n	Electron density
n_0	Electron density in equilibrium [10^{12} cm^{-3}]
J_n	Electron flux in the organic layer
I	electrical current density
E_t	Energy of the interfacial level
ΔE_t	Deepness of Et, with respect to Ec [0.2 eV]
θ	The occupancy of the interfacial level
N_I	The total density (per unit area) of interfacial levels [10^{12} cm^{-2}]
v_{12}	The rate of transfer from metal to interfacial level
v_{23}	The rate of transfer from interfacial to bulk level.
k_{12}	The rate constant for transfer from metal to interfacial level [100 s^{-1}]
k_{23}	The rate constant for transfer from interfacial to bulk level [100 cm^{-3} s^{-1}]
α_1	The asymmetry factor for transfer from metal to interfacial level [0.1]
α_2	The asymmetry factor for transfer from interfacial to bulk level [0.9]

In squares brackets are given the numerical simulation values used in Fig. 3.

$$C_d V_d - C_{sc} V_{sc} = N_I q\theta \qquad (10)$$

Solving Eqs. (5), (9), and (10) we obtain an expression for the potential across the dipole layer in terms of V and θ:

$$V_d = \left\{ -(\varepsilon^2/w_0^2 - 2C_d N_I q\theta) + [(\varepsilon^2/w_0^2 - 2C_d N_I q\theta)^2 - 4C_d^2(N_I^2 q^2 \theta^2 - \varepsilon^2(V - V_{bi})/w_0^2)]^{1/2} \right\} / (2C_d^2). \qquad (11)$$

2.2. Minority carrier generation and dynamics in the organic layer

For the photovoltaic model we use the standard approach that assumes diffusion–recombination–generation in the quasi-neutral region and collection of all the photogenerated minorities in the SCR (no recombination and flat Fermi level) of the organic layer [23,32,33]. Here we discuss the case of illumination from the barrier side, which gives Gärtner's model as a limit, and the correspondent formulas for illumination from the neutral side (see Fig. 1a) are given the Appendix A.

For $w \leqslant x \leqslant L$ we have

$$\frac{\partial^2 n}{\partial x^2} - \frac{n - n_0}{L_n^2} + \frac{\alpha \Phi}{D_n} e^{-\alpha x} = 0 \qquad (12)$$

However, instead of the standard boundary condition ($n = n_0$ at $x = \infty$), considering the limited thickness of the organic layer, we as-

sume a reflecting boundary for electrons at the contact to the neutral region

$$\left. \frac{\partial n}{\partial x} \right|_{x=L} = 0 \qquad (13)$$

Eq. (13) is supported by impedance spectroscopy measurements that show the correspondent spectra [34] and will be reported elsewhere. The solution of Eqs. (12) and (13) is

$$n = n_0 + R\cosh\left(\frac{x - w}{L_n}\right) + S\sinh\left(\frac{x - w}{L_n}\right) + \gamma_n e^{-\alpha x} \qquad (14)$$

where

$$\gamma_n = \frac{L_n^2 \alpha \Phi}{D_n(1 - L_n^2 \alpha^2)} \qquad (15)$$

$$R = n(w) - n_0 - \gamma_n e^{-\alpha w} \qquad (16)$$

$$S = \frac{\alpha L_n \gamma_n e^{-\alpha L}}{\cosh y_L} - R\tanh y_L \qquad (17)$$

$$y_L = \frac{L - w}{L_n} \qquad (18)$$

The electron flux at the edge of the SCR is

$$J_n(w) = -D_n \left.\frac{\partial n}{\partial x}\right|_{x=w} = \frac{D_n}{L_n}\left(-\frac{\alpha L_n \gamma_n e^{-\alpha L}}{\cosh y_L} + R\tanh y_L\right) + \alpha D_n \gamma_n e^{-\alpha w} \qquad (19)$$

In the SCR ($0 \leqslant x \leqslant w$) we have

$$\frac{\partial J_n}{\partial x} = \alpha \Phi e^{-\alpha x} \qquad (20)$$

Integrating Eq. (20) we obtain

$$J_n(0) = J_n(w) + \Phi(e^{-\alpha w} - 1) \qquad (21)$$

The concentration of electrons at both edges of the space-charge region is related by

$$n(w) = n(0)e^{-qV_{sc}/k_BT} \qquad (22)$$

Inserting Eqs. (16), (19), and (22) in (21) we obtain the relation between electron flux and concentration at the edge of the organic layer:

$$J_n(0) = -J_g + \frac{D_n}{L_n}\tanh y_L \left(n(0)e^{-qV_{sc}/k_BT} - n_0\right) \qquad (23)$$

$$J_g = \Phi\left[1 - e^{-\alpha w} + \frac{L_n^2 \alpha^2}{1 - L_n^2 \alpha^2}\left(\frac{e^{-\alpha L}}{\cosh y_L} - \frac{1}{L_n \alpha}\tanh y_L e^{-\alpha w} - e^{-\alpha w}\right)\right] \qquad (24)$$

Let us consider some simplifications of this model. If the metal/organic interface is reversible to electrons ($E_{F1} = E_{Fn}(0)$) [31] and if we assume that $V_d = 0$ then

$$n(0) = n_0 e^{-qV_{bi}/k_BT} \qquad (25)$$

Hence Eq. (23) gives the diode model

$$J_n(0)^{(rev)} = -J_g + \frac{D_n n_0}{L_n}\tanh y_L \left(e^{-qV/k_BT} - 1\right) \qquad (26)$$

In the particular case in which $L \gg L_n$, we obtain

$$J_n(0)^{(rev,\infty)} = -J_g^{(\infty)} + \frac{D_n n_0}{L_n}\left(e^{-qV/k_BT} - 1\right) \qquad (27)$$

$$J_g^{(\infty)} = \Phi\left(1 - \frac{1}{1 + L_n \alpha}e^{-\alpha w}\right) \qquad (28)$$

Eq. (27) then gives Gärtner's model [23]. However, in order to explain the shift of MS plots under illumination with respect to their value in the dark, we assume that the electron transfer at the interface is kinetically limited by a surface state that becomes

charged by photogeneration [15]. This is the next piece of the model that we describe in the following paragraph, and it will be coupled with the general expression for the electron flux at the interface, Eq. (23).

2.3. Transfer of electrons at the metal/organic interface

The model of carrier transfer at the metal–organic interface has been described in previous publications [25–27]. The injection from the metal Fermi level (E_{F1}) to the organic conductor LUMO (E_c), or viceversa, occurs sequentially, via interface states with energy

$$E_t = E_c(0) - \Delta E_t \tag{29}$$

and fractional occupancy θ, see Fig. 1c. However, in the previous papers [25–27], the potential in the dipole layer was assumed to vary linearly with the applied voltage, for simplicity. Here, a new development is that we consider self-consistently the electrostatic conditions at the interface as described in Eq. (11).

Since the trap level E_t varies when V_d changes, we need to determine E_t as a function of voltage. First we note from Fig. 1a

$$E_c = E_{F0} + \zeta_c - q(\phi - \phi_{sc,b}) \tag{30}$$

being

$$\zeta_c = k_B T \ln(N_c/n_0) \tag{31}$$

Therefore,

$$E_c(0) = E_{F0} + \zeta_c - qV_{sc} \tag{32}$$

Hence

$$E_t = E_{F0} + \zeta_c - qV_{sc} - \Delta E_t \tag{33}$$

We obtain

$$E_t - E_{F1} = q(V_{bi} + V_d) + \zeta_c - \Delta E_t \tag{34}$$

On the other hand, for the electron density in the organic layer we have

$$n = N_c e^{-(E_c - E_{Fn})/k_B T} \tag{35}$$

Therefore the position of the electron Fermi level in the SCR is

$$E_{Fn} = E_c(w) + k_B T \left[\frac{n_0}{N_c} + \frac{L_n}{D_n \tanh y_L}(J_n(0) + J_{ph}) \right] \tag{36}$$

The rate of charge transfer between the metal and interfacial states is given by the expression [25]

$$J_{12} = N_l k_{12}\{(1 - \theta)A - \theta B\} \tag{37}$$

where

$$A = \exp\left[(\alpha_1 - 1)(E_t - E_{F1})/k_B T\right] \tag{38}$$
$$B = \exp\left[\alpha_1(E_t - E_{F1})/k_B T\right] \tag{39}$$

Note that the argument of the exponent in these two equations is determined by Eq. (34). Similarly, the rate of charge transfer between the interface level and the bulk organic material is

$$J_{23} = N_l k_{23}\{N_c \theta C - n(0)(1 - \theta)H\} \tag{40}$$

where

$$C = \exp\left[-\alpha_2 \Delta E_t/k_B T\right] \tag{41}$$
$$H = \exp\left[(1 - \alpha_2)\Delta E_t/k_B T\right] \tag{42}$$

It should be remarked that Eqs. (38) and (39), and separately Eqs. (41) and (42), respectively satisfy the detailed balance conditions [25].

2.4. Solution of the model

In steady state we must have

$$J_{12} = J_{23} = J_n(0) \tag{43}$$

We solve $J_{23} = J_n(0)$ to eliminate n(0) and we obtain

$$J_n(0) = N_l k_{23} \frac{N_c C - \frac{L_n}{D_n}(1 - \theta)He^{qV_{sc}/k_B T}\left(\frac{J_g}{\tanh y_L} + \frac{D_n n_0}{L_n}\right)}{1 + N_l k_{23} \frac{L_n(1 - \theta)He^{qV_{sc}/k_B T}}{D_n \tanh y_L}} \tag{44}$$

The condition $J_{12} = J_{23}$ is solved numerically for $\theta(V)$. Inserting this into Eq. (44), gives the (photo)current as a unique function of the bias voltage V. The electrical current density is defined $I = -qJ_n(0)$. The low frequency capacitance does not contain a contribution from surface states dynamics and is given by the expression

$$C_0^{-1} = C_d^{-1} + C_{sc}^{-1} \tag{45}$$

3. Experimental

Cells with the structure ITO/PEDOT:PSS/P3HT:PCBM/Al were built following the next procedure. The P3HT:PCBM (1:0.8, w/w) solutions were prepared in pure good solvent (Dichlorobenzene) and stirred for 48 h under N_2 conditions. Photovoltaic cells were fabricated under ambient conditions according to the standard device fabrication procedure [35]: first, a 40 nm thick poly(ethylenedioxythiophene):poly(styrene sulfonate) (PEDOT:PSS) layer was spin coated onto a well-cleaned glass substrate covered with a 100 nm thick layer of indium tin oxide (ITO). Secondly, the photoactive layer was fabricated by depositing the prepared solution via spin coating. The resulting thickness of the photoactive layer was around 120 nm. Finally, the devices were completed by the evaporation of 80 nm Al back electrode at pressure lower than 10^{-6} mbar.

The impedance measurements, both in darkness and under illumination of approximately 1.5 AM, were carried out in a high-vacuum chamber, that was integrated in an inert atmosphere (<0.1 ppm O_2 and H_2O) glovebox. The capacitance measurements were performed with an Autolab PGSTAT-30 equipped with a frequency analyzer module at a fixed frequency of 1 kHz. Ac oscillating amplitude was as low as 10 mV (rms) to maintain the response linearity.

The PV devices exhibited photoresponse behaviour when illuminated by a UV filtered halogen lamp typical for these materials in the described device layout with Al cathodes, namely: V_{oc} = 0.39 V, I_{sc} = 8.7 mA cm^{-2}, FF = 42%.

4. Results and discussion

Results of the capacitance measurements of the ITO/PEDOT:PSS/P3HT:PCBM/Al solar cell as a function of bias voltage are shown in Fig. 2. The capacitance behavior is similar to that described previously [11]. At potential negative to the built-in voltage the C^{-2} characteristic is linear, following MS behavior. At further reverse bias the organic layer becomes fully depleted and the capacitance levels off to the geometric value. Above Vbi (flatband potential), the capacitance decreases due to what we believe are limitations to injection [11]. However, this domain is outside the scope of the model described above and will not be considered further in this work. Under illumination, the C^{-2} characteristic displays the same behavior though the flatband potential is shifted negatively by 0.6 V. The levels of p-doping extracted from MS analysis are similar in both cases, light and dark, and are of the order of 5×10^{16} cm^{-3}.
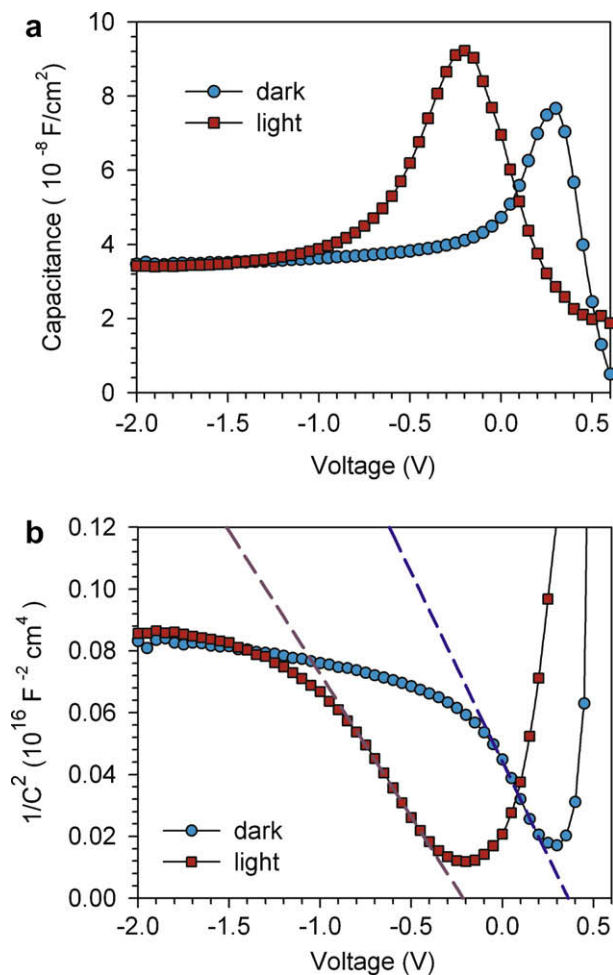
Fig. 2. Experimental plots of capacitance ($1/C^2$) versus voltage in a ITO/PEDOT:PSS/P3HT:PCBM/Al solar cell (effective area of 1.87 cm^2), in dark and under illumination. The capacitance is measured at the frequency 1 kHz, with the indicated bias voltage applied at the ITO contact. The dashed lines are linear fits in the portion obeying Mott–Schottky behavior, with the parameters $V_{bi} = 0.362$ V, $N_A = 3.85 \times 10^{16}$ cm^{-3} (dark), $V_{bi} = -0.215$ V, $N_A = 5.08 \times 10^{16}$ cm^{-3} (light).

As described in the Introduction, the shift of MS plots under illumination is interpreted here as a result of band unpinning by charging a surface state at the metal/organic contact. Following the model of Fig. 1, under illumination, there is an accumulation of minority carriers (with respect to dark conditions), which produces an increase of the quasi-Fermi level E_{Fn} and an additional charge in the surface state. An important requirement for such an additional charging is a slow kinetics of charge transfer through the surface state [24]. The additional charge at the surface state produces an increase of the voltage in the dipole layer, and a displacement of the apparent flatband potential [15]. A similar interpretation was mentioned also in Ref. [12].

These effects can be appreciated in model simulations shown in Fig. 3 using the theory developed above in Section 2. Fig. 3a and b shows current density-potential curves. The slow kinetics of electron removal from the metal/organic interface implies that the curve under light conditions departs strongly from the ideal diode model, Eq. (27), in which the photogeneration current is added to the dark current. In contrast, the current at moderate voltage negative to V_{bi}, is severely limited [22], due to small size of the SCR that increases the charge recombination. The significance of the limitation to extraction has been already pointed out before [9,36]. The model of Glatthaar et al. [9], although with a different approach, already showed the kink in the $I–V$ curve as found here

in Fig. 3b. Figure 3c shows the striking difference between the surface state occupation in dark and illumination conditions, and also the progressive increase of V_d, which occurs at the expense of the depletion layer voltage, and therefore displaces the MS characteristic by about 0.6 V, as shown in Fig. 3d.

The simulation in Fig. 3 provides a reasonable explanation of the relevant trends observed in the experimental results, Fig. 2, and indicate the significance of the surface states in energetics, kinetics, and photovoltaic performance of P3HT:PCBM organic blends. It is worth noting that crucial parameter values able to reproduce the observed shift in the MS plot are the slow charge transfer kinetics used in the simulations of Fig. 3 ($k_{12} = 100$ s^{-1}, and $k_{23} = 100$ cm^{-3} s^{-1}). Fast values entail a collapse of the MS plot under illumination into the dark characteristics. The deepness of the surface state with respect to the LUMO level ΔE_t has a linear effect on the MS shift. In addition, the order of magnitude of the dipole layer capacitance C_d and that of the SCR C_{sc} should coincide. In case of $C_d \gg C_{sc}$, the dipole layer absorbs the whole potential drop
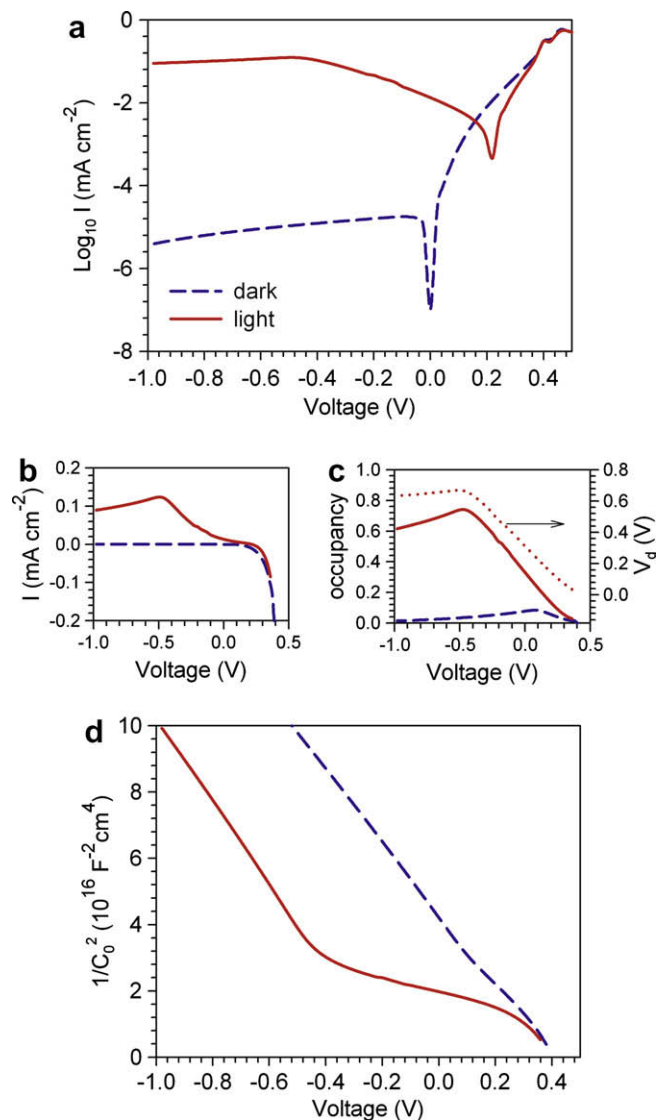
Fig. 3. Numerical simulations of the photovoltaic model of generation–diffusion limited by interfacial surface state kinetics discussed in the text, with parameter values given in Table 1. Several quantities are shown for dark and under photon irradiation with respect to voltage (negative to V defined in Fig. 1). (a) Current density potential curve in semilog and (b) linear representation. (c) Occupancy of the surface state, and potential drop across the dipole layer. (d) Capacitance in $1/C^2$ representation.

and the MS characteristic is not observable. Another determining parameter is the electron diffusion length L_n. For high recombination cells $L_n < 100$ nm, the MS shift is still reproduced but the surface state ability to be charged is limited. Other parameters have been chosen in accordance to values usually reported.

We have not attempted a quantitative analysis of all the aspects of the experimental results. Obviously, due to the complexity of this kind of device the model contains a significant number of parameters governing the operation of the solar cell. To asses this fully a variety of experimental methods are required to extract the diffusion length, the diffusion coefficient of minority carriers, etc. This study is currently in progress in our laboratories. In addition, the model of Section 2 may require extension in several well-known aspects, e.g. recombination in space-charge region, distribution in energy of the surface states [27], and recombination at the surface state by hole capture.

5. Conclusions

A detailed analysis of capacitance characteristics in P3HT:PCBM solar cells indicates a considerable displacement of the band under illumination. A basic photovoltaic model accounting for the essential characteristics of the system indicates that surface states with a slow exchange kinetics, become charged under illumination. This modifies the energetics of the electron extraction contact and constitutes a major factor limiting the performance of bulk heterojunction solar cells.

Acknowledgments

Appendix A. Illumination from the neutral side

$$\frac{\partial^2 n}{\partial x^2} - \frac{n - n_0}{L_n^2} + \frac{\alpha \Phi}{D_n} e^{\alpha(x-L)} = 0 \tag{46}$$

$$n = n_0 + R \cosh\left(\frac{x-w}{L_n}\right) + S \sinh\left(\frac{x-w}{L_n}\right) + \gamma_n e^{\alpha(x-L)} \tag{47}$$

$$R = n(w) - n_0 - \gamma_n e^{\alpha(w-L)} \tag{48}$$

$$S = -\frac{\alpha L_n \gamma_n}{\cosh y_L} - R \tanh y_L \tag{49}$$

$$J_n(w) = \frac{D_n}{L_n}\left(R \tanh y_L + \frac{\alpha L_n \gamma_n}{\cosh y_L}\right) - \alpha D_n \gamma_n e^{\alpha(w-L)} \tag{50}$$

$$J_n(0) = J_n(w) + \Phi e^{-\alpha L}(1 - e^{\alpha w}) \tag{51}$$

$$J_g = \Phi$$
$$\times \left[e^{-\alpha L}(-1 + e^{\alpha w}) + \frac{L_n^2 \alpha^2}{1 - L_n^2 \alpha^2}\left(\frac{\tanh y_L}{L_n \alpha} e^{\alpha(w-L)} - \frac{1}{\cosh y_L} + e^{\alpha(w-L)}\right) \right] \tag{52}$$

References

[1] C.J. Brabec, N.S. Sariciftci, J.C. Hummelen, Adv. Funct. Mater. 11 (2000) 15.
[2] W. Ma, C. Yang, X. Gong, K.-S. Lee, A.J. Heeger, Adv. Funct. Mater. 15 (2005) 1617.
[3] C. Tanase, E.J. Meijer, P.W.M. Blom, D.M. de Leeuw, Phys. Rev. Lett. 91 (2003) 216601.
[4] P. Vanlaeke et al., Thin Solid Films 511–512 (2006) 358.
[5] V.D. Mihailetchi, H. Xie, B. de Boer, L.J.A. Koster, P.W.M. Blom, Adv. Funct. Mater. 16 (2007) 699.
[6] W. Osikowicz, M.P. de Jong, W.R. Salaneck, Adv. Mat. 19 (2007) 4213.
[7] M.S.A. Abdou, F.P. Orfino, Y. Son, S. Holdcroft, J. Am. Chem. Soc. 119 (1997) 4518.
[8] S. Hoshino, M. Yoshida, S. Uemura, T. Kodzasa, N. Takada, T. Kamata, K. Yase, J. Appl. Phys. 95 (2004) 5088.
[9] M. Glatthaar et al., Sol. Energy Mater. Sol. Cells 91 (2007) 390.
[10] D.B.A. Rep, A.F. Morpurgo, T.M. Klapwijk, Org. Electron. 4 (2003) 201–207.
[11] G. Garcia-Belmonte, A. Munar, E.M. Barea, J. Bisquert, I. Ugarte, R. Pacios, Org. Electron. 9 (2008) 847.
[12] E.J. Meijer, A.V.G. Mangnus, C.L. Huisman, G.W. t'Hooft, D.M. de Leeuw, T.M. Klapwijk, Synth. Met. 142 (2004) 53.
[13] A.M. Cowley, J. Appl. Phys. 37 (1966) 3024.
[14] E.H. Rhoderick, R.H. Williams, Metal-Semiconductor Contacts, Clarendon Press, Oxford, 1988.
[15] J.J. Kelly, R. Memming, J. Electrochem. Soc. 192 (1982) 730.
[16] C.R. Crowell, G.I. Roberts, J. Appl. Phys. 40 (1969) 3726.
[17] C. Barret, A. Vapaille, J. Appl. Phys. 50 (1979) 4217.
[18] J. Werner, A.F.J. Levi, R.T. Tung, M. Anzlowar, M. Pinto, Phys. Rev. Lett. 60 (1988) 53.
[19] P. Allongue, H. Cachet, G. Horowitz, J. Electrochem. Soc. 130 (1983) 2352.
[20] P. Allongue, H. Cachet, J. Electrochem. Soc. 132 (1985) 45.
[21] J. Li, L.M. Peter, J. Electroanal. Chem. 199 (1986) 1.
[22] J. Li, L.M. Peter, J. Electroanal. Chem. 193 (1985) 27.
[23] W. Gärtner, Phys. Rev. 116 (1959) 84.
[24] J. Reichman, Appl. Phys. Lett. 36 (1980) 574.
[25] J. Bisquert, G. Garcia-Belmonte, A. Pitarch, H. Bolink, Chem. Phys. Lett. 422 (2006) 184.
[26] G. Garcia-Belmonte, H. Bolink, J. Bisquert, Phys. Rev. B 75 (2007) 085316.
[27] G. Garcia-Belmonte, J. Bisquert, P.R. Bueno, C.F.O. Graeff, Chem. Phys. Lett. 455 (2008) 242.
[28] A. Pitarch, K. Meerholz, D. Hertel, Phys. Stat. Sol. (a) 245 (2008) 814.
[29] D. Vanmaekelbergh, Electrochim. Acta 42 (1997) 1121.
[30] S. Södergren, A. Hagfeldt, J. Olsson, S.E. Lindquist, J. Phys. Chem. 98 (1994) 5552.
[31] J. Bisquert, D. Cahen, S. Rühle, G. Hodes, A. Zaban, J. Phys. Chem. B 108 (2004) 8106.
[32] F. El Guibaly, K. Colbow, B.L. Funt, J. Appl. Phys. 52 (1981) 3480.
[33] J. Nelson, The Physics of Solar Cells, Imperial College Press, London, 2003.
[34] J. Bisquert, J. Phys. Chem. B 106 (2002) 325.
[35] B.C. Thompson, J.M. Fréchet, Angew. Chem. Int. Ed. 47 (2008) 58.
[36] I. Mora-Seró, J. Bisquert, Sol. Energy Mater. Sol. Cells 85 (2005) 51.